Modeling and optimization of a solar forward osmosis pilot plant by response surface methodology

M. Khayet[a, b, *], J.A. Sanmartino[a], M. Essalhi[a], M.C. García-Payo[a], N. Hilal[c]

[a] Department of Applied Physics I, Faculty of Physics, University Complutense of Madrid, Spain
[b] Madrid Institute for Advanced Studies of Water (IMDEA Water Institute), Avda. Punto Com, n_ 2, 28805, Alcalá de Henares, Madrid, Spain
[c] Centre for Water Advanced Technologies and Environmental Research (CWATER), College of Engineering, Swansea University, Swansea SA2 8PP, UK

Abstract

Forward osmosis (FO) is a water treatment/separation technology of emerging interest. Due to its complex nature involving various operating parameters, modeling of this separation process is challenging. A solar thermal and photovoltaic-powered FO pilot plant has been optimized by means of a statistical experimental design and response surface methodology. Predictive models were developed for simulation and optimization of different responses such as the water permeate flux, the reverse solute permeate flux and the FO specific performance index that includes the water and reverse solute permeate fluxes together with the energy consumption. The considered input variables of the FO pilot plant were the feed flow rate, the permeate flow rate and the temperature. The developed response models have been tested using the analysis of variance. A Monte Carlo Simulation method has been conducted to determine the optimum operating conditions of the FO pilot plant. The obtained optimum parameters were confirmed experimentally. Regeneration of the draw solution can be performed by means of an optimized solar powered reverse osmosis (RO) pilot plant with an optimum FO specific performance index ranging from 25.79 to 0.62 L/g kW h achieved under the FO optimal conditions, 0.83 L/min feed flow rate, 0.31 L/min draw solution flow rate and 32.65 °C temperature. The FO energy consumption is only 14.1% the total energy consumption of the FO/RO hybrid system.

Keywords: Forward osmosis; Solar energy; Optimization; Reverse osmosis; Design of experiment; Response surface methodology; Desalination; Water treatment

*Corresponding author at: Department of Applied Physics I, Faculty of Physics, University Complutense of Madrid, Spain.

Nomenclature

A	effective membrane area (m^2)
B	vector of the regression coefficients (β)
C	NaCl salt concentration (g/L)
E	energy consumption (kW h)
F	ratio of variances
N	number of experimental runs
N	number of factors (independent variables)
P	pressure (Pa)
R^2	coefficient of multiple determination
R_{adj}^2	adjusted statistic coefficient
T	temperature (°C)
T	operating time (s)
U	number of significant regression coefficients in the RSM model
V	volume (m^3)
X	($N \times u$) matrix of the independent variables
x_i	coded value of the operating variables
Y	($N \times 1$) vector of the experimental response
$\hat{Y}$	predicted response as a function of the coded variables (x_i)
Z	actual value of the operating variable

Subscripts

F	feed
Max	maximum
Min	minimum
P	permeate or draw solution
S	solute (salt NaCl)
Sp	specific
Tab	tabulated
W	water

Superscripts

0	center point

Greek letters

A	star or axial point for the orthogonal CCD (= ±1.215 for 3 variables)
B	regression coefficients (in Eq. (10))
E	statistical error in the RSM model
Φ	flow rate (L/min)
Π	osmotic pressure (Pa)

Abbreviations

ANOVA	analysis of variances
CCD	central composite design
DF	degree of freedom
DoE	design of experiments

RSM	response surface methodology
MS	mean square
SS	sum of squares

1. Introduction

Membrane technologies experienced important developments during last decades allowing significant increases in water production with high quality and low energy consumption. These are attributed mainly to a wide range of available advanced materials, novel and efficient technologies as well as to the well known increasing demand of water supply and sanitation. The worldwide renewed interest in the osmotically driven membrane processes such as forward osmosis (FO) and pressure retarded osmosis (PRO) has increased tremendously in the last few years (Achilli and Childress, 2010, Alsvik and Hägg, 2013, Ge et al., 2013, Gormly, 2014, Helfer et al., 2014, Lutchmiah et al., 2014, Schrier, 2012 and Shaffer et al., 2015).

Osmosis is the transport of water across a semi-permeable water selective membrane from a feed solution of higher water chemical potential to a solution of lower water chemical potential (i.e. higher osmotic pressure or higher salt concentration) known as a draw solution. The membrane ideally permits the passage of water rejecting solute(s) molecules or ions. Fig. 1 shows four possible situations that can occur when a semi-permeable water selective membrane is placed in direct contact with pure water and a saline aqueous solution given here as an example. Once water starts moving through the membrane, the hydrostatic pressure at the permeate side of the membrane becomes higher than that of the feed side, resulting in a transmembrane hydrostatic pressure (ΔP) higher than zero. The water flux stops when ΔP equals the osmotic pressure difference ($\Delta\pi$) established between the feed and the permeate. This is the pressure which, if applied to the saline solution, would prevent transport of water across the membrane.

FO occurs when the only transmembrane driving force for water flux is the osmotic pressure difference ($\Delta\pi$) (see Fig. 1). In other words, no transmembrane hydrostatic pressure is applied ($\Delta P = 0$). In this case a high concentration solution (i.e. draw solution) is separated from a low concentration solution by a water selective semi-permeable membrane. The concentration gradient between both the feed and draw solution induces a transmembrane $\Delta\pi$. Consequently, water flows spontaneously through the membrane from the low concentration side to the draw solution side. In FO mode, generally both the feed solution to be treated and the draw solution are circulated tangentially to each side of the membrane module. The used membranes have an asymmetric structure consisting of an active dense or porous layer with pore sizes below 10 nm and a support layer. Various types of osmotic solutions are considered (i.e. sucrose, glucose, $MgCl_2$, $CaCl_2$, NaCl, KCl, etc.) (Cai et al., 2013 and Ge et al., 2013). Some advantages of FO are its potential low energy consumption (i.e. electric energy) to run the circulation pumps as well as its high rejection of a wide range of contaminants. One of the problems of FO is the reverse permeate flux of the draw solute, which must be minimal. FO is being applied in various separation processes such as in wastewater treatment, food processing, seawater or brackish water desalination (Gormly, 2014, Lutchmiah et al., 2014, Schrier, 2012 and Shaffer et al., 2015).

PRO is an intermediate process between FO and the well known reverse osmosis (RO) technology, where the hydraulic pressure is applied in the opposite direction of the osmotic

pressure gradient. In this case, water from a low salinity aqueous solution permeates through a semi-permeable water selective membrane into a pressurized high salinity solution (i.e. seawater). The additional water volume increases the pressure in the permeate side of the PRO membrane module. The power (termed also osmotic power) is then obtained by depressurizing the permeate through, for example, a hydro-turbine. PRO is similar to RO, but in PRO process the applied pressure is maintained below $\Delta\pi$. It must be pointed out that when the applied ΔP is lower than $\Delta\pi$ (Fig. 1), the water permeate flux is still driven by $\Delta\pi$ in the direction of the concentrated draw solution. The interesting application area of PRO is the generation of electricity (Achilli and Childress, 2010 and Helfer et al., 2014). When the applied hydrostatic pressure ΔP is greater than $\Delta\pi$ (Fig. 1), the direction of the water flux is reversed leading to the well-known RO separation process used mainly in seawater desalination (Attia, 2012, Delgado-Torres and García-Rodríguez, 2012, Khayet et al., 2010a and Manolakos et al., 2009). Since 1990s the development of low pressure (i.e. high permeability) RO membranes has progressed rapidly (Elimelech and Phillip, 2011 and Khayet et al., 2010a).

FO technology is still in continuous improvements trying to overcome the many faced challenges and barriers in order to extend its fields of industrial application. As stated previously, the growing interest of FO is attributed mainly to its lower energy consumption compared to other technologies and to its wider possibility to be coupled to other separation processes including RO for water production and regeneration of the used draw solution (Altaee et al., 2014, Blandin et al., 2015, Choi et al., 2009, Luo et al., 2014, Martinetti et al., 2009, McGovern and Lienhard, 2014, Schrier, 2012 and Zhang et al., 2014). It is worth quoting that actual improvements of FO technology, that can contribute to more competitive FO plants achieving significant reductions of energy consumption and water production cost, are focused on the development of FO fouling resistant membranes with low internal concentration polarization coefficients (*ICP*), the design of non-toxic draw solutions with higher osmotic pressures, the combination of FO installation to solar energy systems and the optimization of FO operating factors. As far as we know still there is no published paper on the utilization of renewable energy sources such as wind energy and solar energy systems (i.e. thermal collectors and photovoltaic panels, PV) to run FO plants. Schrier (2012) used solar evaporation for regeneration of the draw solution by removing excess of water using FO for production of fuel-grade ethanol. It is also noted that all the studies reported so far on FO deal with the conventional method of experimentation, in which the effect of an operation variable on the FO system performance is investigated keeping the other variables fixed. This classical or conventional method of experimentation requires many experimental runs, which take a lot of time especially for FO pilot plant tests, ignores the interaction effects between the operating parameters and leads to a low efficiency in optimization resulting in a high energy consumption. These limitations of the classical method of experimentation can be avoided by applying the response surface methodology (RSM) that involves statistical design of experiments (DoE) in which all factors are varied simultaneously over a set of experimental runs. In fact, RSM is a collection of mathematical and statistical techniques useful for developing, improving and optimizing processes, and can be used to evaluate the relative significance of several affecting factors even in the presence of complex interactions between them using a minimum number of experiments (Khayet et al., 2010a, Montgomery, 2001 and Montgomery and Myers, 1995). In this methodology, all factors are simultaneously varied between minimum and maximum values. It is worth quoting that RSM has been applied successfully in various scientific and technical fields (Cojocaru et al., 2009a, Cojocaru et al., 2009b, Kacan, 2015, Khayet et al., 2007, Khayet et al., 2010a, Khayet et al., 2010b, Khayet et al., 2011a, Schenone et al., 2015, Zamani et al., 2015 and Ai et al., 2015). In the present study, the central composite experimental design (CCD) and RSM has been applied to model and

optimize a solar FO pilot plant. The objective is to ensure a high water production rate of the FO pilot plant with a low reverse solute permeability and reduced energy consumption.

2. Experimental

2.1. Description of the solar FO pilot plant

A schematic diagram of the FO pilot plant used for experimental design is shown in Fig. 2. It is equipped with a commercial spiral wound membrane module (2521FO-CS, Hydration Technology Innovation LLC, HTI, Albany, OR, USA) having an effective membrane area of 0.35 m^2. This is fabricated using a corrugated spacer (CS) with 2.5 mm polystyrene chevron design flow path and the membrane 120629-ES-2(CTA-ES). The temperature limit of the membrane as indicated by the manufacturer (HTI) is 0–43 °C. The membrane housing is Axeon 2521 PVC and GTX material (AXEON Water Technologies, Temecula, USA). The maximum differential pressure through the side ports of the feed solution (outlet and inlet of the feed solution) is recommended to be below 50 kPa. The maximum pressure of the draw solution entering the end port of the membrane module is recommended to be 70 kPa. The feed and draw solution circulates tangentially to the membrane surfaces in a co-current configuration. The FO plant consists of feed and permeate double wall containers, two circulation pumps (Totton magnetically coupled centrifugal pumps DC 40/0, 12 V DC 12 A) connected to each container. As can be seen in Fig. 2, the pilot plant is equipped with vents, temperature sensors, pressure gauges, flow-meters, etc.. The temperatures and pressures were measured at the inlets and outlets of the membrane module by Pt100 sensors connected to a digital multimeter (FLUKE HYDRA) and manometers (Wika, 0–250 kPa), respectively. The flow rates of the feed and permeate were recorded by pulse flow controllers (RS 511-3892). The temperatures of the circulating liquids were adjusted through glass heat exchangers. The energy consumption of the circulation pumps, thermostat and the whole FO pilot plant (electrical and thermal) were measured independently by means of Velleman NETBSEM2 (wattage 5–4416 W) apparatus.

The operating variables of the FO pilot plant are the flow rate of the feed aqueous solution (ϕ_F), the flow rate of the draw solution or permeate (ϕ_P) and the inlet temperature of both the feed and permeate (T). The feed inlet pressure (P_F), the permeate inlet pressure (P_P) and the initial concentration of the draw solution (C_p) were maintained the same. In this study, the used draw solution is a saline aqueous solution of 35 g/L (NaCl) and the inlet feed and permeate pressures were kept below 30 kPa.

To carry out the first part of the study dealing with experimental design, either a thermostat (Tamson Holland, Type: TX 3/150, Gomensoro S.A.) was used to maintain the inlet temperature between 31 °C and 42 °C or a cryostat (Polyscience Recirculator, Hz/A/Ph: 50/5.6/1) for lower temperatures than 31 °C. In the second part of the study, the temperature of the feed and permeate solution were controlled by coupling a solar thermal collector to the containers of the FO pilot plant through their jackets and glass heat exchangers permitting to adjust the temperature at the required value. The solar thermal collector has a spherical geometry with a diameter of 1.05 m and an effective collection area of 4 m^2. The absorber plate is made of copper with a selective coating layer of titanium oxide. The whole collector is protected by a methacrylate cover of 3 mm thickness. The liquid solution used for heat transfer is made of water and glycol with a working temperature range of −10 °C to 100 °C. The collector contains an internal thermal tank made of stainless steel (AISI 304) coated with polyurethane with a capacity of 150 L. Inside the tank, there is a heat exchanger, also made of

stainless steel. The hydraulic circuit of the collector is connected to a circulation pump (40 W). The controller unit Multical 401 provided by the company Kamstrup (Germany) was used to record the temperatures as well as the liquid flow-rates. An automatic data acquisition system (SAD, DC-100, Yogagawa) was used to record every 5 s the temperatures using Pt-100 sensors and the liquid flow-rate. A pyranometer (Skye-TORN) was employed to measure the global irradiation on horizontal plane. More details may be found in Khayet et al. (2010a).

The two circulation pumps (for feed and permeate in Fig. 2) working on DC voltage were run by a set of 3 batteries (Master Vision AGM, MV100Ah–12V) powered by a PV flat panel (monocrystalline silicon of 33 Wp). In order to minimize the heat loss of the FO pilot plant, the membrane module, the containers and pipes were insulated.

The water permeate flux (J_W) was determined by recording the height (i.e. volume) variation (ΔV) of both the feed and permeate during a predetermined time (Δt = 30 min in this study). This can be calculated from:

$$J_W = \frac{\Delta V}{A \Delta t} \qquad \text{equation (1)}$$

where A is the effective membrane area.

The salt concentrations of the feed or retentate and permeate were determined in real time by a calibrated electrical conductivimeter (Ω Metrohm) every 30 min. The reverse solute permeate flux (J_S) can be calculated for a predetermined time from the concentration (C_F) and volume (V_F) of the feed solution using the following equation:

$$J_S = \frac{\Delta (C_F V_F)}{A \Delta t} \qquad \text{equation (2)}$$

2.2. Experimental statistical design

The statistical design of experiments (DoE) is a structured method of experimentation in which all factors are varied simultaneously. In this study an orthogonal central composite design (CCD) with star points was employed with 3 factors and 5 levels. Table 1 shows the controllable variables (i.e. factors) and their levels in actual and coded values calculated as follows:

$$x_i = \frac{z_i - z_i^0}{\Delta z_i} \quad \forall\ i = 1, 2, 3 \qquad \text{equation (3)}$$

$$z^0 = \frac{z_{max} + z_{min}}{2} \qquad \text{equation (4)}$$

$$\Delta z = \frac{z_{max} - z_{min}}{2} = z_{max} - z^0 = z^0 - z_{min} \qquad \text{equation (5)}$$

where z is the actual value of the operating variable, x is the coded value, z_{max} is the maximum actual value corresponding to x = +1, z_{min} is the actual minimum value corresponding to x = −1

and the subscript *i* refers to the feed flow rate, ϕ_F (i = 1), draw solution flow rate, ϕ_P (i = 2) and the inlet temperature, T (i = 3).

The CCD design consists of 16 experiments with 8 orthogonal design points (i.e. factorial points), 6 star points to form the central composite design with α = ±1.215 and 2 center points for replication. α is the star point in the experimental design that gives the limits of the valid region of experimentation, Ω [$x_j \in \Omega$; $\Omega = \{x_j | -\alpha \leqslant x_j \leqslant +\alpha\}$; $\forall j$ = 1, 2, 3]. The experimental design matrix is summarized in Table 2. The 8 top experiments in this table correspond to the orthogonal design, the 6 following are the axial experiments with "star points" to form the central composite design and finally the last two experiments are replicate experiments to estimate the experimental error for each response. Each experimental run was performed for 4 h and the volumes (i.e. heights of the feed and permeate containers) together with the salt concentrations of the feed and draw solution, their flow rates, temperatures and pressures were registered with time together with the energy consumption.

Fig. 3 shows as an example the determined permeate flux (J_W) from the volume of the permeate container. The decrease of J_W with time is not linear due to the reduction of the salt concentration of the draw solution indicating that the dilution of the draw solution is not negligible in this case. The high permeate fluxes correspond to the runs 1 and 13, which were carried out applying the highest temperatures (40–41.94 °C) and moderate/high feed and permeate flow rates (0.300–0.779 L/min). In contrast, the lowest permeate fluxes were observed for the runs 6 and 8, which corresponds to the lowest temperature (22 °C) and the lowest feed and permeate flow rates (0.094–0.121 L/min). In order to determine the average permeate flux J_W of each experimental run, $J_W(t)$ was first fitted to the following polynomial regression equation:

$$J_W(t) = a_0 + a_1 t + a_2 t^2 + a_3 t^3 \qquad \text{equation (6)}$$

where the regression coefficients a_0, a_1, a_2 and a_3 were computed via the least square method. All the experimental data were fitted well with reasonably high correlation coefficients (i.e. $R^2 > 0.972$). Then the average permeate flux J_W was calculated as:

$$J_W = \frac{1}{t_n} \int_{t_1}^{t_n} J_W(t) dt \qquad \text{equation (7)}$$

where t_1 is the initial time, 30 min in this study, and t_n is the final time, 4 h. The results are summarized in Table 2.

The reverse solute flux (J_S) was calculated using Eq. (2). Providing that the variation of ($C_F V_F$) is not linear with time, the average value of J_S was determined following the same procedure as J_W (i.e. regression analysis using Eqs. (6) and (7)). It was also noted that the variation with time of the salt concentration of both the feed (C_F) and permeate (C_P) aqueous solutions were not linear. The obtained average value of J_S for each experimental run is also reported in Table 2. During any FO process there is a loss of the draw solute due to the reverse solute permeate flux (J_S) and the ratio (J_W/J_S), termed the reverse solute flux selectivity, must be maximized (Shaffer et al., 2015).

In this study, the output responses of the FO pilot plant are J_W, J_S, the ratio (J_W/J_S), the total energy consumption (E_c), the specific water permeate flux ($J_{W,sp}$) defined as:

$$J_{W,sp} = \frac{J_W}{E_c} \qquad \text{equation (8)}$$

and the specific FO performance index (Y_{sp}) defined as:

$$Y_{sp} = \frac{J_W}{J_S E_c} \qquad \text{equation (9)}$$

It is worth quoting that in FO process, J_W must be high whereas J_S and E_c must be as low as possible. Providing that $J_{W,sp}$ does not take into consideration J_S, Y_{sp} was used as response, since it takes into consideration J_W, J_S and E_c and must be as high as possible.

3. Results and discussions

3.1. RSM models

FO experiments have been carried out according to the experimental design summarized in Table 2. The obtained results (responses) are also presented in Table 2.

The RSM models have been developed for the responses, J_W, J_S, J_w/J_S, $J_{W,sp}$ and Y_{sp} defined in the previous section. Each response has been linked to the coded factors x_1, x_2 and x_3 by a 2nd order polynomial model with interactions as shown in the following equation (Montgomery and Myers, 1995, Khayet et al., 2007 and Khayet et al., 2010b):

$$\widehat{Y} = \beta_0 + \sum_{i=1}^{k} \beta_i x_i + \sum_{i=1}^{k} \beta_{ii} x_i^2 + \sum_{j} \sum_{i=1\,(i<j)}^{k} \beta_{ij} x_i x_j + \varepsilon \qquad \text{equation (10)}$$

where $\widehat{Y}$ <img height="17" border="0" style="vertical-align:bottom" width="13" alt="View the MathML source" title="View the MathML source" src="http://origin-ars.els-cdn.com/content/image/1-s2.0-S0038092X16303048-si1.gif">Y^ is the predicted response, x_i and x_j ($j = k + 1$, $i < j$) are the coded independent variables (factors), β_0, β_1, … , β_k, β_{ij} are the regression coefficients and ε is the statistical error.

The regression coefficients of the RSM model were computed by means of Multiple Linear Regression (MLR) method in order to minimize the sum of squares of the residuals. The least square estimations of the regression coefficients were calculated by the following matrix equation (Montgomery and Myers, 1995, Ismail and Lai, 2004, Khayet et al., 2007 and Khayet et al., 2010b):

$$B = (X^T X)^{-1} X^T Y \qquad \text{equation (11)}$$

where B is the vector formed by the regression coefficients, X is the matrix ($N \times u$) of the independent variables, u is the number of regression coefficients in the RSM model (Eq. (10)) and Y is a vector ($N \times 1$) formed by the responses of the N experiments. According to this method the β coefficients are determined by the method of least squares (i.e. the β values are

chosen in order to minimize the sum of squared residuals). For each response, first the regression coefficients using the coded variables have been determined. Subsequently, the regression coefficients corresponding to the actual variables have been calculated as shown below.

3.1.1. RSM model of the water permeate flux (J_W)

The obtained regression equation of J_W in terms of the coded variables is:

$$\widehat{Y} = 5.2261 + 0.3692x_1 + 0.0547x_2 + 0.676x_3 - 0.6733x_2^2 - 0.1387x_3^2 + 0.056x_1x_2 + 0.0666x_1x_3 + 0.1414x_2x_3 \quad \text{equation (12)}$$

The regression coefficients were tested for significance using Student's *t*-test. Therefore, in the above equation only the significant coefficients were maintained. The regression coefficient b_{11} is found to be negligible. The empirical model obtained in terms of actual parameters is determined and written in general form as follows:

$$J_W = 0.3741 + 0.177\phi_F + 7.0492\phi_P + 0.1483T - 15.8662\phi_P^2 - 1.7123 \cdot 10^{-3}T^2 + 0.8263\phi_F\phi_P + 0.0225\phi_F T + 0.0763\phi_P T \quad \text{equation (13)}$$

where 0.050 L/min $\leqslant \phi_F \leqslant$ 0.850 L/min; 0.050 L/min $\leqslant \phi_P \leqslant$ 0.550 L/min and 20.07 °C $\leqslant T \leqslant$ 41.94 °C.

The RSM model was validated statistically for adequacy by analysis of variance (ANOVA) and the obtained results are summarized in Table 3. The statistical significance of the second-order regression model was determined by *F*-value, which is a measurement of variance of data about the mean, based on the ratio of mean square of group variance due to error. If the model gives a good prediction of the experimental data then the calculated *F*-value should be greater than the tabulated *F*-value, 3.8 in this case. For the RSM model of J_W, the calculated *F*-value is found to be much greater than 3.8 (i.e. three variables). This means that the developed model is valid from statistical standpoint and it is a good predictor of the experimental data. Moreover, the R^2-value is 0.9828, which is desirable. This implies that more than 98.28% of the data deviation can be explained by the developed empirical model. Furthermore, the predicted R^2 values are in agreement with the adjusted statistics R^2_{adj}. This means that only significant terms have been included in the empirical model. All the above cited statistical estimators show that the RSM model for J_W is statistically accepted for prediction of J_W in a wide range of the valid region of experimentation. Fig. 4 presents the comparison of J_W calculated by the RSM model and the experimental one obtained in each test (Table 2). This comparison shows a good agreement between the predicted J_W values and the corresponding experimental ones.

The effects of the FO operating variables on J_W are shown in Fig. 5. The curves were obtained using the RSM model (Eq. (13)). It can be seen the gradual increase of J_W with the increase of both ϕ_F and T for all values of ϕ_P. These results are due to the reduction of the thickness of the feed boundary layer with the increase of ϕ_F leading to lower polarization effect and to the increase of both the solubility and diffusivity membrane parameters with the increase of T (Xie et al., 2013). However, a maximum J_W is observed with the variation of ϕ_P for all ranges of ϕ_F and T. The increase of J_W up to a maximum with the increase of ϕ_P is due to the reduction of both temperature and concentration polarization effects. The increase of ϕ_P reduced the external concentration polarization effect and therefore increased both J_W and J_S. The

subsequent decline of J_W may be attributed to the rapid loss of the draw solute of the permeate for higher ϕ_P values.

3.1.2. RSM model of the reverse solute permeate flux (J_S)

The developed RSM model of J_S in terms of the coded variables is:

$$\widehat{Y} = 3.14 - 0.1757x_1 - 0.1191x_2 - 0.0326x_3 + 0.1534x_1^2 - 0.1943x_2^2 + 0.0491x_3^2 + 0.0615x_1x_2 \quad \text{equation (14)}$$

The regression coefficients corresponding to the interaction terms b_{13} and b_{23} are found to be negligible. In terms of the actual variables the RSM model is written as:

$$J_S = 4.246 - 2.0818\phi_F + 1.7607\phi_P - 0.0412T + 1.4172\phi_F^2 - 4.5787\phi_P^2 + 6.0617 \cdot 10^{-4}T^2 + 0.9074\phi_F\phi_P \quad \text{equation (15)}$$

where 0.050 L/min $\leqslant \phi_F \leqslant$ 0.850 L/min; 0.050 L/min $\leqslant \phi_P \leqslant$ 0.550 L/min and 20.07 °C $\leqslant T \leqslant$ 41.94 °C.

The RSM model was validated statistically for adequacy by means of ANOVA and the results are summarized in Table 4. The calculated *F*-value is found to be greater than the tabulated one and the R^2-value (0.9737) is greater than R^2_{adj} indicating that the developed RSM model for J_S is valid from statistical standpoint and only the significant terms have been considered in the model. As can be seen in Eqs. (14) and (15), the only interaction term affecting J_S is the feed and permeate flow rates (b_{12}). The other interactions between parameters are negligible. In addition, compared to ϕ_F and ϕ_P, the effect of the temperature on J_S is less significant. A comparison between the J_S response calculated by the RSM model and the experimental one obtained in each test (Table 2) is plotted in Fig. 6. A good agreement was found between both responses.

The effects of the three variables (ϕ_F, ϕ_P and T) on J_S are shown in Fig. 7. The increase of ϕ_F clearly leads to a strong reduction of J_S tending to asymptotic values and therefore, as it is required by FO process, the solute flux selectivity (J_W/J_S) is high. As can be seen in Fig. 5 and Fig. 7, the effects of ϕ_P on J_S and J_W are similar. Interestingly it was observed an increase of J_W/J_S with the increase of T and ϕ_F for all ϕ_P values. However, for low values of T and ϕ_F the ratio J_W/J_S increased up to a maximum with the increase of ϕ_P and then decreased; whereas for high values of T and ϕ_F it shows a continuous gradual increase attributed meanly to the much higher J_W compared to that of J_S.

3.1.3. RSM model of the specific FO performance index (Y_{sp})

The specific FO performance index (Y_{sp}) that takes into account all FO responses (J_W, J_S, E_c) was calculated by means of Eq. (9). The obtained RSM model of Y_{sp} is as follows in terms of the coded variables:

$$\widehat{Y} = 2763.6 + 213.3881x_1 + 424.8272x_3 - 460.5659x_2^2 - 1249.1x_3^2 \quad \text{equation (16)}$$

The regression coefficient b_2, b_{11} and all the interaction terms b_{12}, b_{13} and b_{23} are found to be negligible. In terms of the actual variables, the RSM model is written as:

$$Y_{sp} = -1.4788 \cdot 10^4 + 648.596\phi_F + 6.5119 \cdot 10^3 \phi_P + 1003.3T - 1.0853 \cdot 10^4 \phi_P^2 - 15.421T^2 \quad \text{equation (17)}$$

where 0.050 L/min $\leqslant \phi_F \leqslant$ 0.850 L/min; 0.050 L/min $\leqslant \phi_P \leqslant$ 0.550 L/min and 20.07 °C $\leqslant T \leqslant$ 41.94 °C.

The response surface model was validated statistically for adequacy by ANOVA. The results are presented in Table 5. The calculated F-value is greater than 3.8 and the R^2-value is reasonably high (i.e. 0.9679). This R^2 value is in agreement with the adjusted statistics R^2_{adj} indicating that only significant terms have been included in the RSM model of the FO response Y_{sp}. These statistical estimators show that the RSM model of Y_{sp} is valid from statistical standpoint and it is a good predictor of the experimental data. Fig. 8 shows the comparison of the response Y_{sp} calculated by the RSM model and the experimental one obtained in each test (Table 2). A good agreement can be seen between the predicted Y_{sp} values and the corresponding experimental data.

The effects of the operating FO variables on the response Y_{sp} are plotted in Fig. 9. The increase of T and ϕ_P results in an enhancement of Y_{sp} up to a maximum, and then for higher values the trends are declined suggesting the existence of an optimal Y_{sp} value. It is to be noted that the effect of T upon Y_{sp} is the most significant one especially for high ϕ_F values. It can be observed a gradual increase of Y_{sp} with the increase of ϕ_F for all T and ϕ_P ranges. This result is due to the reduction of the polarization effect (i.e. narrowing of the feed boundary layer thickness) and the subsequent enhancement of the ratio J_W/J_S for practically the same energy consumption (E_c).

It was also observed that the effects of the FO operating parameters on the specific water permeate flux ($J_{W,sp}$) calculated by means of Eq. (8) are similar to those observed for the response Y_{sp}. In fact, the regression coefficient b_2, b_{11} and all the interaction terms b_{12}, b_{13} and b_{23} were also found to be negligible.

3.2. Optimization of the FO pilot plant

One of the main objectives of this study is to determine the optimum operating conditions of the FO pilot plant in order to maximize the specific FO performance index (Y_{sp}) (i.e. maximize J_W, J_W/J_S and $J_{W,sp}$ and minimize J_S and E_c). This has been performed by means of Monte Carlo Simulation (MCS) method, which is a stochastic optimization technique that generates the random coded values of the input FO variables and correspondingly generates a response inside the valid experimental region (Cojocaru et al., 2009a, Cojocaru et al., 2009b, Khayet et al., 2011a and Khayet et al., 2011b). 13 optimal points were obtained and the mean values of the optimum variables together with their standard deviations are summarized in Table 6 in terms of the actual operating variables as well as the predicted value of Y_{sp}. The experimental confirmation run was carried out under the optimum operating variables and the Y_{sp} response deviates only 0.7% from the predicted value. This experimental value of Y_{sp} together with that of the test number 9 (Table 2) represent the best (maximal) values throughout all the conducted experimental tests inside the region of experimentation.

The other experimental data of this optimum point are 2.94 g/m^2 h for J_S, 5.81 L/m^2 h for J_W, 1.976 L/g for J_W/J_S and 12.55 L/g kW h for $J_{W,sp}$. These responses were also predicted by the developed RSM models of each response and the obtained values were quite similar to the experimental ones (i.e. 3.14 g/m^2 h for J_S, 5.80 L/m^2 h for J_W, 1.850 L/g for J_W/J_S and 13.32 L/g kW h for $J_{W,sp}$).

3.3. Solar-powered FO pilot plant operation under optimum conditions

The FO solar-powered pilot plant is investigated under the determined optimal operating condition given in Table 6. It should be noted that the connection between the solar heat spherical collector and the feed and permeate aqueous solutions has been designed in such way to ensure a fixed temperature throughout the required testing period required. Fig. 10 shows as an example the instantaneous global solar radiation on horizontal plane (I) and the adjusted temperature (T) for the solar FO pilot plant to the determined optimum value during the entire period of experimentation together with the calculated responses J_W, J_S, $J_{W,sp}$ and Y_{sp}. Except this last response, the other three responses are reduced with the operating time due to the dilution of the draw solution reducing the FO driving force. As a consequence, the calculated response Y_{sp} is reduced quickly after 30 min of operation of the FO pilot plant (i.e. 79.6%) reaching then a minimum value of 20.19 L/g kW h at 3 h 15 min operation time and then is increased. The determined values of Y_{sp} are higher than those obtained without using solar systems (Table 2 and Fig. 8 and Fig. 9). This is expected due to the considered energy consumption of the used thermostats or cryostat to carry out the designed experimental runs. Since the solar FO pilot plant is autonomous and operates without using thermostat or cryostat, energy consumption has been reduced. Therefore, Y_{sp} values plotted in Fig. 10(c) are higher than those presented in Fig. 9(c).

Because of the dilution of the draw solution, another separation process such as membrane distillation (MD) (Khayet, 2011, Martinetti et al., 2009 and Zhang et al., 2014) or RO (Altaee et al., 2014 and Blandin et al., 2015) can be used as a second step for draw solution regeneration and water production. In this study the solar RO pilot plant detailed elsewhere (Khayet et al., 2010a) is considered under optimum conditions forming a hybrid FO/RO plant as schematized in Fig. 11. In order to maintain constant the salt concentration of the draw solution, the RO water permeate flux must be similar to the FO permeate flux. As an example, the determined responses for a typical sunny day are plotted in Fig. 12. As can be seen J_W, J_S and $J_{W,sp}$ are maintained almost the same (i.e. 7.1 ± 0.4 L/m^2 h for J_W, 3.6 ± 0.4 g/m^2 h for J_S and 8.5 ± 0.5 L/kW h for $J_{W,sp}$). The observed slight decline of these responses is attributed mainly to the reverse solute. However, Y_{sp} is reduced with time from 25.79 L/g kW h to an asymptotic value 0.62 L/g kW h. This is due to the fact that the ratio J_W/J_S is maintained around a value of 2.0 ± 0.1 L/g whereas the total energy consumption (E_c) of the hybrid FO/RO system is increasing with time. Compared to the Y_{sp} data given in Fig. 10(c), these low values plotted in Fig. 12(c) are attributed to the consideration of the RO energy consumption (Khayet et al., 2010a). For instance, the FO energy consumption is only 14.1 ± 0.2% the total energy consumption of the FO/RO plant. It is to point out that the main benefit of using the FO/RO plant instead of RO plant is the possibility to treat a wide range of wastewater types not only desalination taking advantage of the low energy consumption of FO technology and its lower fouling effects (Altaee et al., 2014, Blandin et al., 2015, Choi et al., 2009 and McGovern and Lienhard, 2014).

4. Conclusions

The statistical design of experiment (DoE) and response surface methodology (RSM) proved to be an useful and effective method for modeling and optimization of a solar FO pilot plant using a minimal number of experimental runs. Predictive RSM models of different FO responses were developed and confirmed their statistical validations by analysis of variance (ANOVA).

The observed gradual increase of J_W with the increase of both ϕ_F and T at all ranges of ϕ_P and the increase of J_W up to a maximum with the increase of ϕ_P, is due to the reduction of the thickness of the feed boundary layer leading to lower polarization effect and to the increase of both the solubility and diffusivity membrane parameters (i.e. permeability) with the increase of T. The increase of ϕ_P reduced the external concentration polarization effect and thus increased both J_W and J_S. The only interaction term affecting J_S is the feed and permeate flow rates ($\phi_F \cdot \phi_P$). Compared to ϕ_F and ϕ_P, the effect of T on J_S is less significant. The increase of ϕ_F clearly leads to a strong reduction of J_S tending to asymptotic values and therefore the solute flux selectivity (J_W/J_S) is high. Interestingly it was observed an increase of J_W/J_S with the increase of T and ϕ_F for all ϕ_P values. However, for low values of T and ϕ_F the ratio J_W/J_S increased up to a maximum with the increase of ϕ_P and then decreased; whereas for high values of T and ϕ_F it shows a continuous gradual increase attributed meanly to the much higher J_W compared to that of J_S.

The increase of T and ϕ_P results in an enhancement of Y_{sp} up to a maximum, and the effect of T upon Y_{sp} is the most significant one especially for high ϕ_F values. A gradual increase of Y_{sp} was observed with the increase of ϕ_F for all T and ϕ_P ranges.

The optimal FO operating variables of the pilot plant corresponding to the maximum of the Y_{sp} were determined by Monte Carlo Simulation (MCS) method. The obtained optimal operational conditions are 0.83 L/min feed flow rate, 0.31 L/min draw solution flow rate and 32.65 °C temperature. By applying these values, maximal Y_{sp} value was predicted and confirmed experimentally.

The FO solar-powered pilot plant was investigated under the determined optimal operation conditions. Except Y_{sp} the other responses of the FO pilot plant (J_W, J_S, $J_{W,sp}$) are reduced with the operating time due to the dilution of the draw solution reducing therefore the FO driving force. The regeneration of the draw solution can be performed by means of an optimized solar powered reverse osmosis (RO) pilot plant with an optimum FO Y_{sp} index ranging from 25.79 to 0.62 L/g kW h achieved under the FO optimal conditions. The FO energy consumption is only 14.1% the total energy consumption of the FO/RO plant.

The solar FO pilot plant has been optimized using 35 g/L NaCl as a draw solution. Similar studies can be applied to any FO plant with other concentrations, feed and draw solutions.

Acknowledgements

The authors wish to thank the financial support of the University Complutense of Madrid, UCM, Banco Santander (Project GR3/14, UCM group 910336) and of the Spanish Ministry of Economy and Competitiveness (Project CTM2015-65348-C2-2R).

References

A. Achilli, A.E. Childress
Pressure retarded osmosis: from the vision of Sidney Loeb to the first prototype installation – review. Desalination, 261 (2010), pp. 205–211

C. Ai, D. Zhou, Q. Wang, X. Shao, Y. Lei
Optimization of operating parameters for photocatalytic degradation of tetracycline using In2S3 under natural solar radiation. Sol. Energy, 113 (2015), pp. 34–42

I. Alsvik, M.B. Hägg
Pressure retarded osmosis and forward osmosis membranes: materials and methods. Polymers, 5 (2013), pp. 303–327

A. Altaee, G. Zaragoza, H. Rost van Tonningen
Comparison between forward osmosis-reverse osmosis and reverse osmosis processes for seawater desalination. Desalination, 336 (2014), pp. 50–57

A.A.A. Attia
Thermal analysis for system uses solar energy as a pressure source for reverse osmosis (RO) water desalination. Sol. Energy, 86 (2012), pp. 2486–2493

G. Blandin, A.R.D. Verliefde, C.Y. Tang, P. Le-Clech
Opportunities to reach economic sustainability in forward osmosis-reverse osmosis hybrids for seawater desalination. Desalination, 363 (2015), pp. 26–36

Y. Cai, W. Shen, S.L. Loo, W.B. Krantz, R. Wang, A.G. Fane, X. Hu
Towards temperature driven forward osmosis desalination using semi-IPN hydrogels as reversible draw agents. Water Res., 11 (2013), pp. 3773–3781

Y.J. Choi, J.S. Choi, H.J. Oh, S. Lee, D.R. Yang, J.H. Kim
Toward a combined system of forward osmosis and reverse osmosis for seawater desalination. Desalination, 247 (2009), pp. 239–246

C. Cojocaru, M. Khayet, G. Zakrzewska-Trznadel, A. Jaworska
Modeling and multi-response optimization of pervaporation of organic aqueous solutions using desirability function approach. J. Hazard. Mater., 167 (2009), pp. 52–63

C. Cojocaru, G. Zakrzewska-Trznadel, A. Jaworska
Removal of cobalt ions from aqueous solutions by polymer assisted ultrafiltration using experimental design approach. Part 1: Optimization of complexation conditions. J. Hazard. Mater., 169 (2009), pp. 599–609

A.M. Delgado-Torres, L. García-Rodríguez
Design recommendations for solar organic Rankine cycle (ORC)-powered reverse osmosis (RO) desalination. Renew. Sustain. Energy Rev., 16 (2012), pp. 44–53

M. Elimelech, W.A. Phillip
The future of seawater desalination: energy, technology, and the environment. Science, 333 (5) (2011), pp. 712–717

Q. Ge, M. Ling, T.S. Chung
Draw solutions for forward osmosis processes: decelopments, challenges, and prospects for the future. J. Membr. Sci., 442 (2013), pp. 225–237

S. Gormly
Forward osmosis: introduction and applications for wastewater processing, energy conservation and energy generation. A. Gugliuzza, A. Basile (Eds.), Membranes for Clean and Renewable Power Applications,. Woodhead Publishing, Cambridge (UK) (2014), pp. 379–395

F. Helfer, C. Lemckert, Y. Anissimov
Osmotic power with pressure retarded osmosis: theory, performance and trends – a review. J. Membr. Sci., 453 (2014), pp. 337–358

A.F. Ismail, P.Y. Lai
Development of defect-free asymmetric polysulfone membranes for gas separation using response surface methodology. Separ. Purif. Tech., 40 (2) (2004), pp. 191–207

E. Kacan
Exergetic optimization of basic system components for maximizing exergetic efficiency of solar combined systems by using response surface methodology. Energy Build., 91 (2015), pp. 65–82

M. Khayet, C. Cojocaru, M.C. García-Payo
Application of response surface methodology and experimental design in direct contact membrane distillation. Ind. Eng. Chem. Res., 46 (2007), pp. 5673–5685

M. Khayet, M. Essalhi, C. Armenta-Déu, C. Cojocaru, N. Hilal
Optimization of solar-powered reverse osmosis desalination pilot plant using response surface methodology. Desalination, 261 (2010), pp. 284–292

M. Khayet, M.N. Abu Seman, N. Hilal
Response surface modelling and optimization of composite nanofiltration modified membranes. J. Membr. Sci., 349 (2010), pp. 113–122

M. Khayet
Membranes and theoretical modelling of membrane distillation: a review. Adv. Colloid Interf. Sci., 164 (2011), pp. 56–88

M. Khayet, A.Y. Zahrim, N. Hilal
Modelling and optimization of coagulation of highly concentrated industrial leather dye by response surface methodology. Chem. Eng. J., 167 (2011), pp. 77–83

M. Khayet, C. Cojocaru, M. Essalhi
Artificial neural network modeling and response surface methodology of desalination by reverse osmosis. J. Membr. Sci., 368 (2011), pp. 202–214

H. Luo, Q. Wang, T.C. Zhang, T. Tao, A. Zhou, L. Chen, X. Bie
A review on the recovery methods of draw solutes in forward osmosis. J. Water Process Eng., 4 (2014), pp. 212–223

K. Lutchmiah, A.R.D. Verliefde, K. Roest, L.C. Rietveld, E.R. Cornelissen
Forward osmosis for application in wastewater treatment: a review. Water Res., 58 (2014), pp. 179–197

D. Manolakos, G. Kosmadakis, S. Kyritsis, G. Papadakis
On site experimental evaluation of a low-temperature solar organic Rankine cycle system for RO desalination. Sol. Energy, 83 (2009), pp. 646–656

C.R. Martinetti, A.E. Childress, T.Y. Cath
High recovery of concentrated RO brines using forward osmosis and membrane distillation. J. Membr. Sci., 331 (2009), pp. 31–39

R.K. McGovern, J.H. Lienhard
On the potential of forward osmosis to energetically outperform reverse osmosis desalination. J. Membr. Sci., 469 (2014), pp. 245–250

Design and Analysis of Experiments. (fifth ed.)John Wiley & Sons, New York (2001)

D.C. Montgomery, R.H. Myers
Response Surface Methodology: Process and Product in Optimization Using Designed Experiments. John Wiley & Sons, New York (1995)

A.V. Schenone, L.O. Conte, M.A. Botta, O.M. Alfano
Modeling and optimization of photo-Fenton degradation of 2,4-D using ferrioxalate complex and response surface methodology (RSM). J. Environ. Manage., 155 (2015), pp. 177–183

J. Schrier
Ethanol concentration by forward osmosis with solar-regenerated draw solution. Sol. Energy, 86 (2012), pp. 1351–1358

D.L. Shaffer, J.R. Werber, H. Jaramillo, S. Lin, M. Elimelech
Forward osmosis: where are we now?. Desalination, 15 (2015), pp. 271–284

M. Xie, W.E. Price, L.D. Nghiem, M. Elimelech
Effects of feed and draw solution temperature and transmembrane temperature difference on the rejection of trace organic contaminants by forward osmosis. J. Membr. Sci., 438 (2013), pp. 57–64

H. Zamani, M. Moghiman, A. Kianifar
Optimization of the parabolic mirror position in a solar cooker using the response surface method (RSM). Renew. Energy, 81 (2015), pp. 753–759

S. Zhang, P. Wang, X. Fu, T.S. Chung
Sustainable water recovery from oily wastewater via forward osmosis-membrane distillation (FO-MD). Water Res., 52 (2014), pp. 112–121

LIST OF FIGURES:

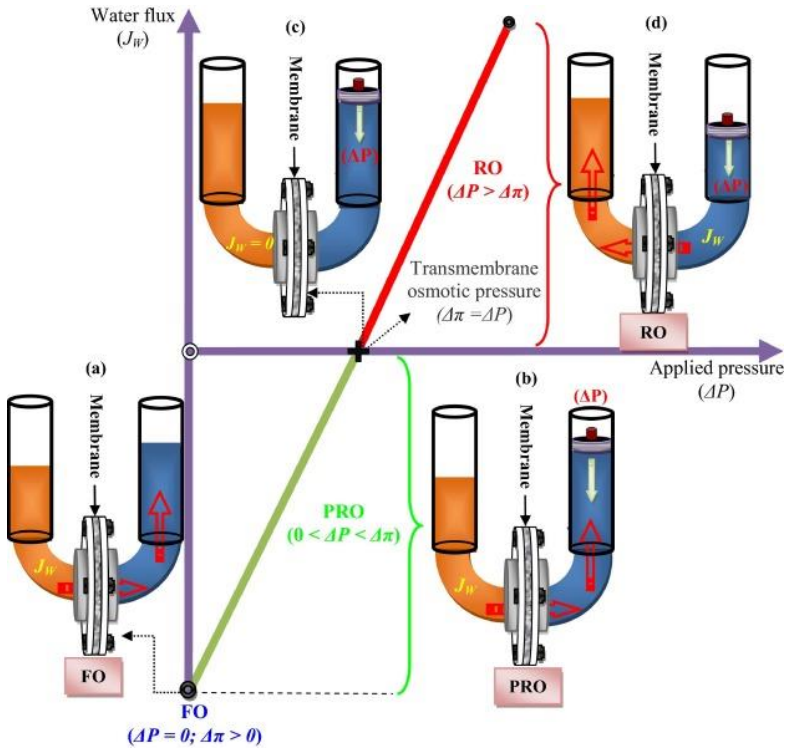

Fig. 1. Schematic presentation of possible osmotic situations showing the water permeate flux (J_w) as a function of the transmembrane hydrostatic pressure (ΔP): (a) FO, (b) PRO, (c) No water permeate flux ($J_w = 0$) and (d) RO.

s.

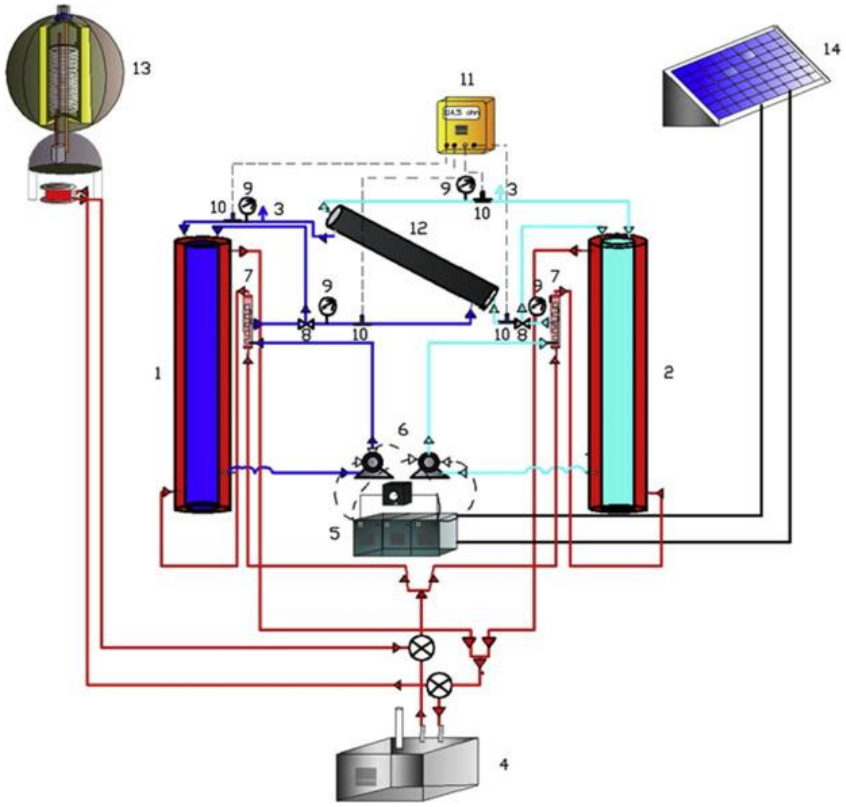

Fig. 2. Basic scheme of the FO pilot plant used to carry out the experimental design: 1-Feed container; 2-Permeate container; 3-Liquid sample collector for analysis; 4-Thermostat; 5-Batteries; 6-Circulation pumps; 7-Heat exchanger; 8-Valves; 9-Manometers; 10-Temperature sensors; 11-Digital multimeter; 12-Membrane module; 13-Thermal solar collector; 14-Photovoltaic panel.

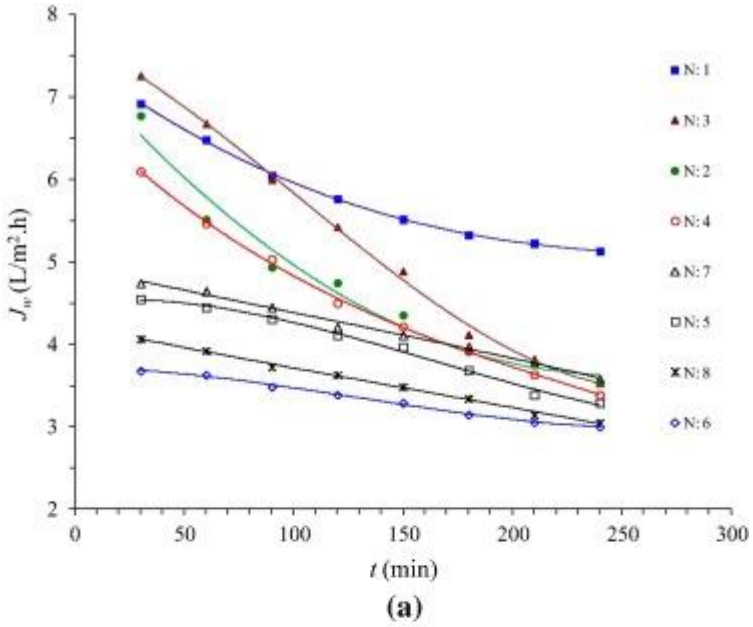

(a)

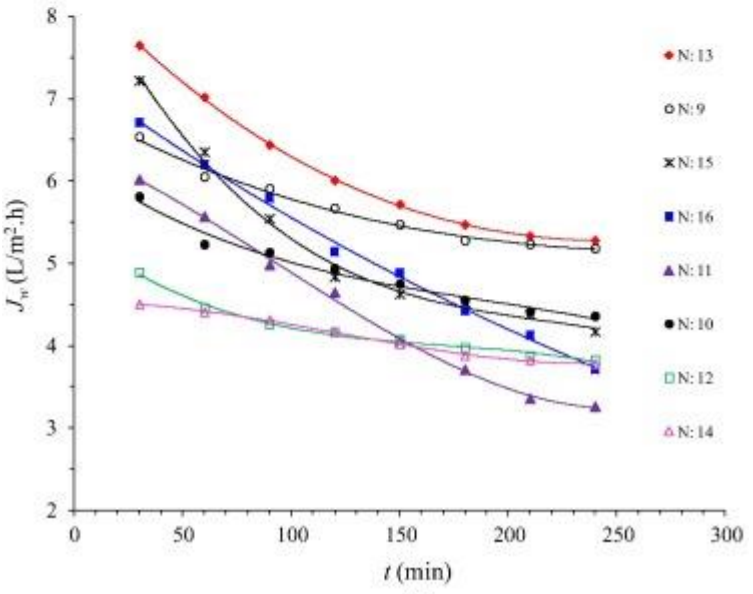

(b)

Fig. 3. FO water permeate flux (J_w) of different experimental runs *versus* time. The solid lines represent the fitting curves to Eq. (6). (a) Orthogonal design tests and (b) axial and center design tests.

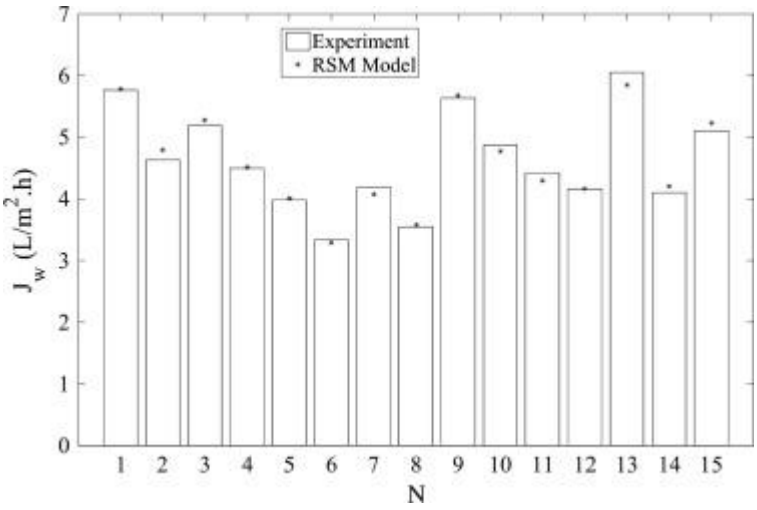

Fig. 4. Experimental and predicted FO water permeate flux (J_w) of different experimental runs indicated in Table 2

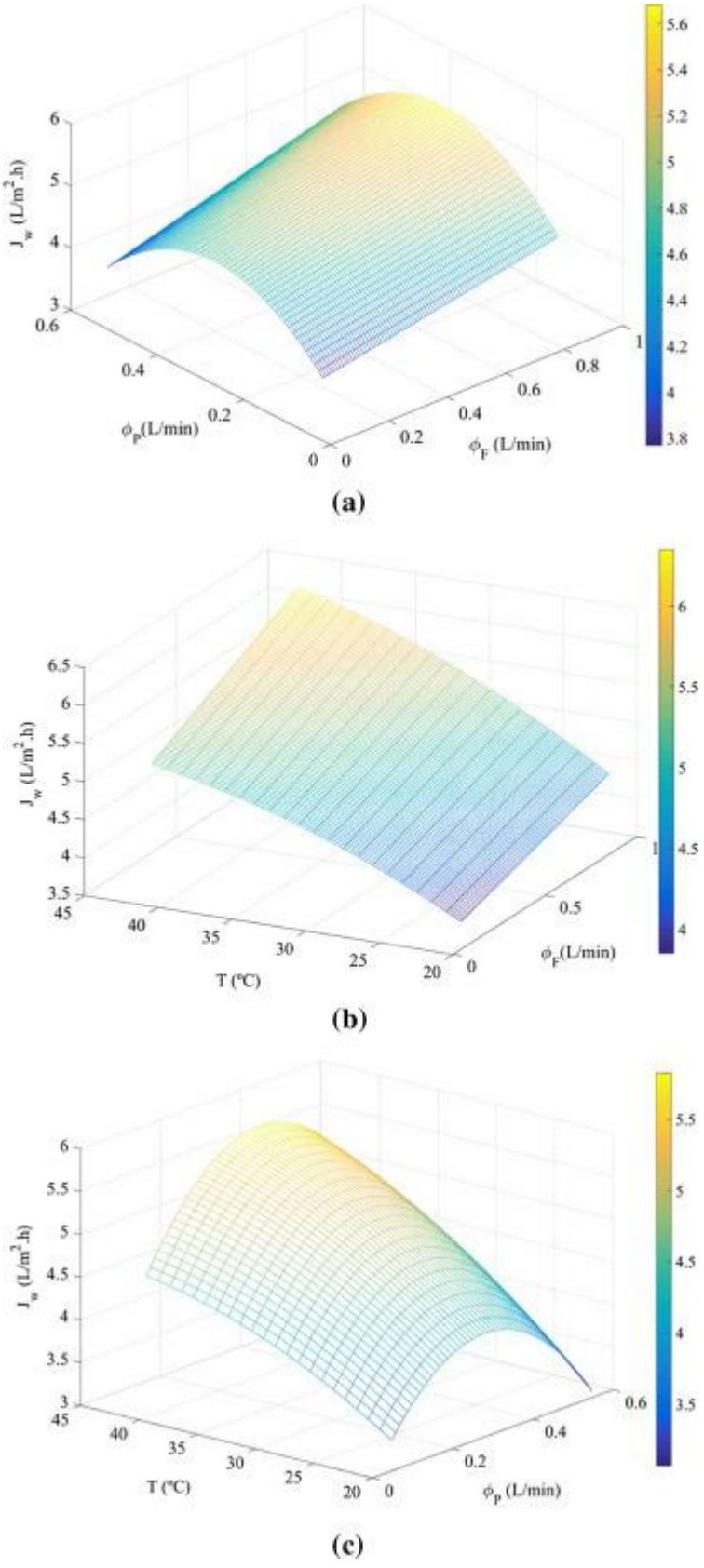

Fig. 5. Response surface plots of the water permeate flux (J_w) as a function of the temperature (T), feed flow rate (ϕ_F) and permeate flow rate (ϕ_P): (a) T = 31 °C; (b) ϕ_P = 0.3 L/min; (c) ϕ_F = 0.45 L/min.

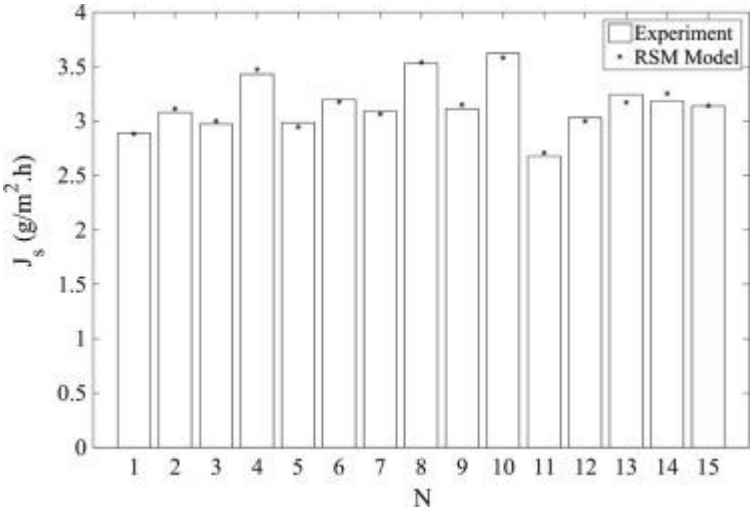

Fig. 6. Experimental and predicted reverse solute permeate flux (J_S) of different experimental runs indicated in Table 2.

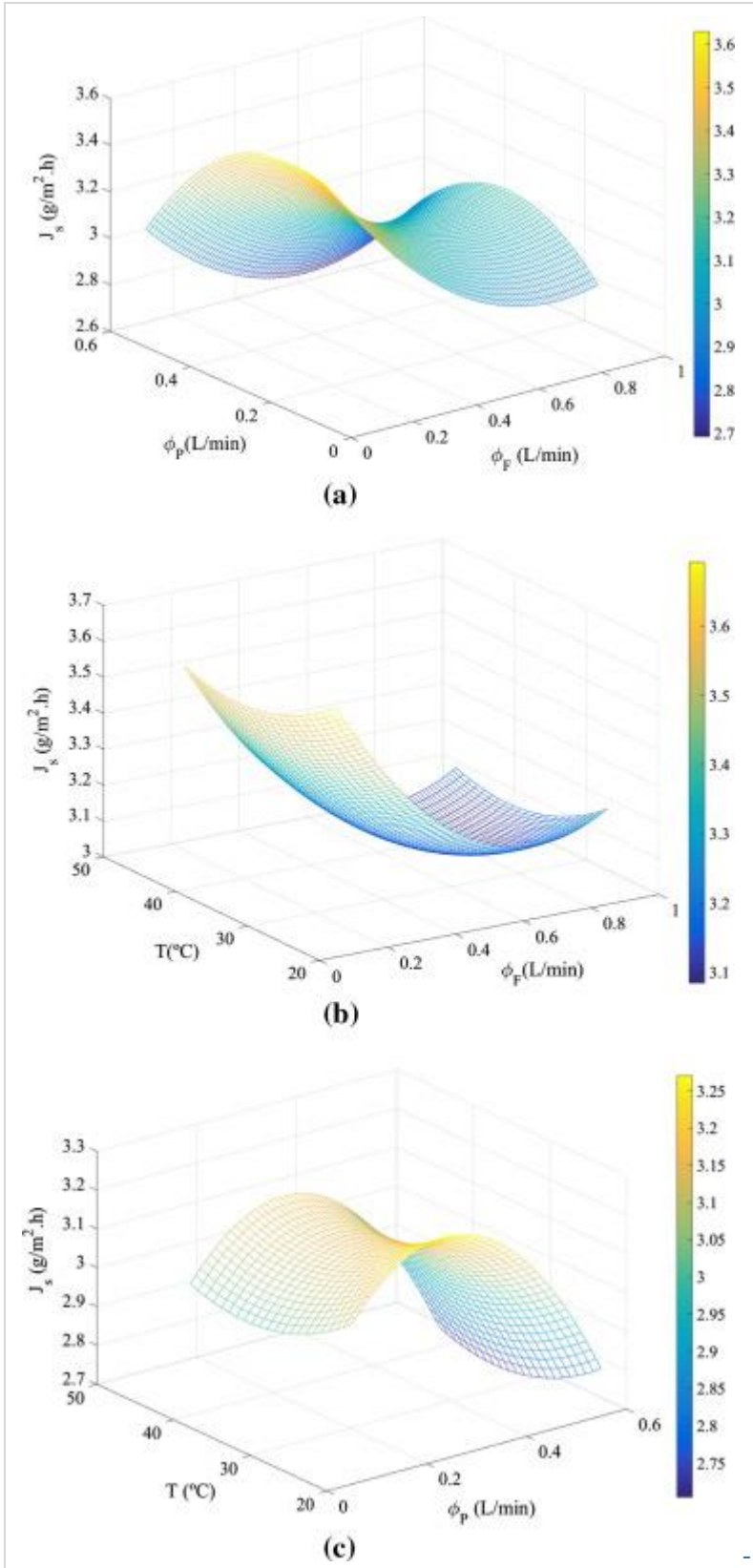

Fig. 7. Response surface plots of the reverse solute permeate flux (J_s) as a function of the temperature (T), feed flow rate (ϕ_F) and permeate flow rate (ϕ_P): (a) T = 31 °C; (b) ϕ_P = 0.3 L/min; (c) ϕ_F = 0.45 L/min

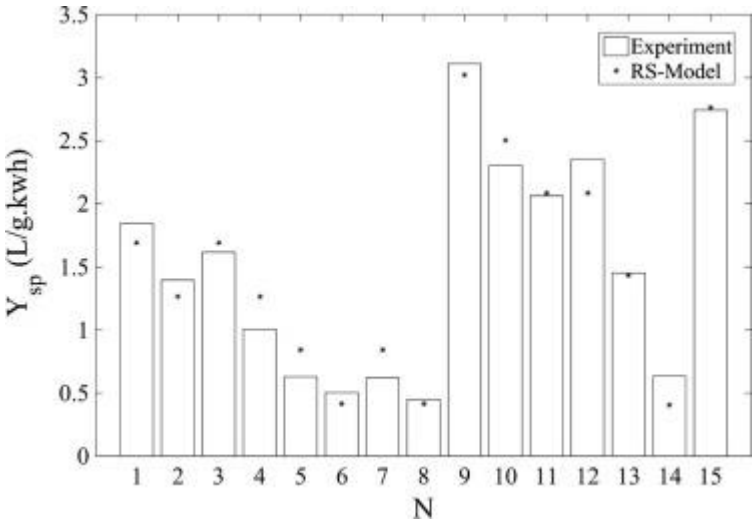

Fig. 8. Experimental and predicted specific FO performance index (Y_{sp}) of different experimental runs indicated in Table 2

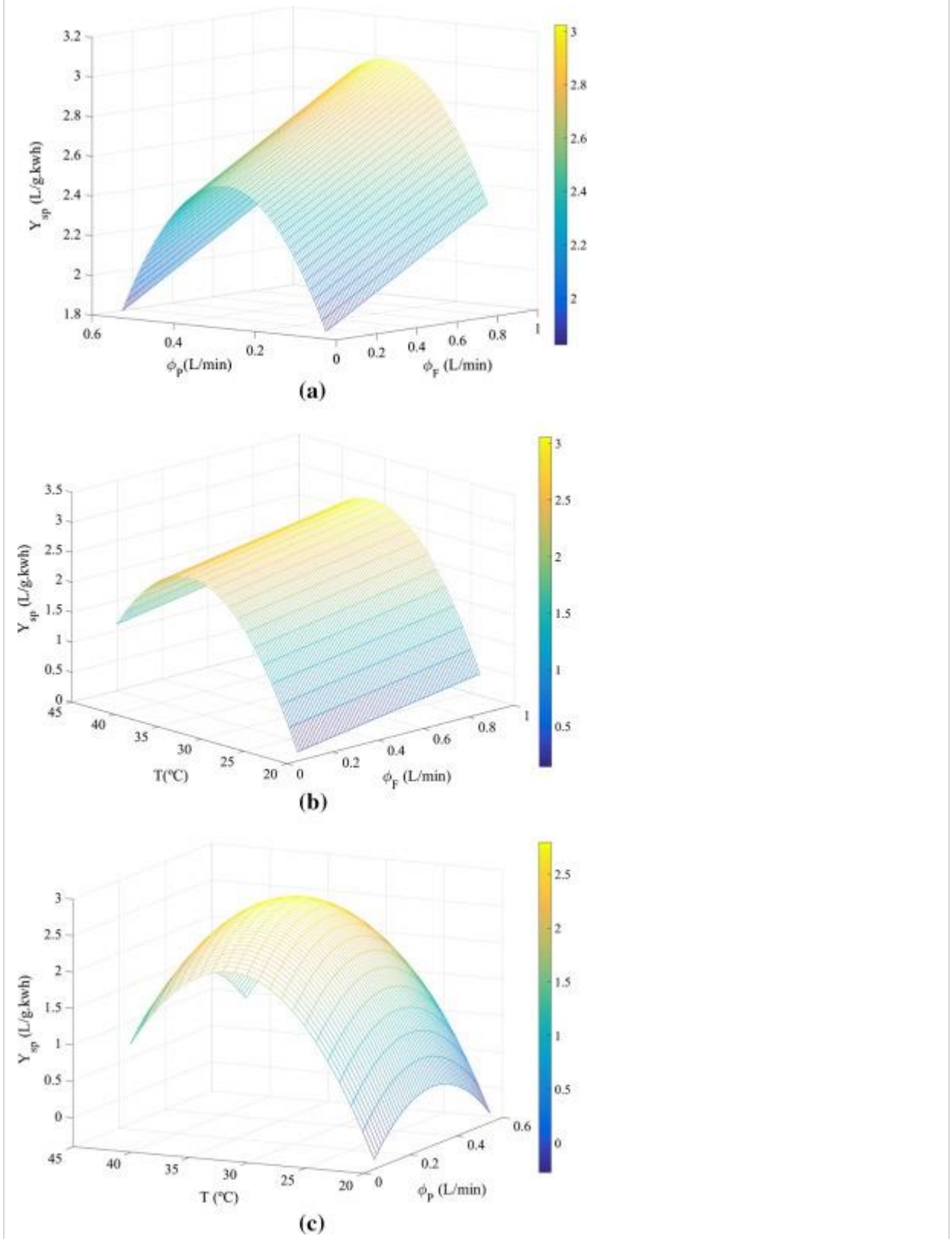

Fig. 9. Response surface plots of the specific FO performance index (Y_{sp}) as a function of the temperature (T), feed flow rate (ϕ_F) and permeate flow rate (ϕ_P): (a) T = 31 °C; (b) ϕ_P = 0.3 L/min; (c) ϕ_F = 0.45 L/min.

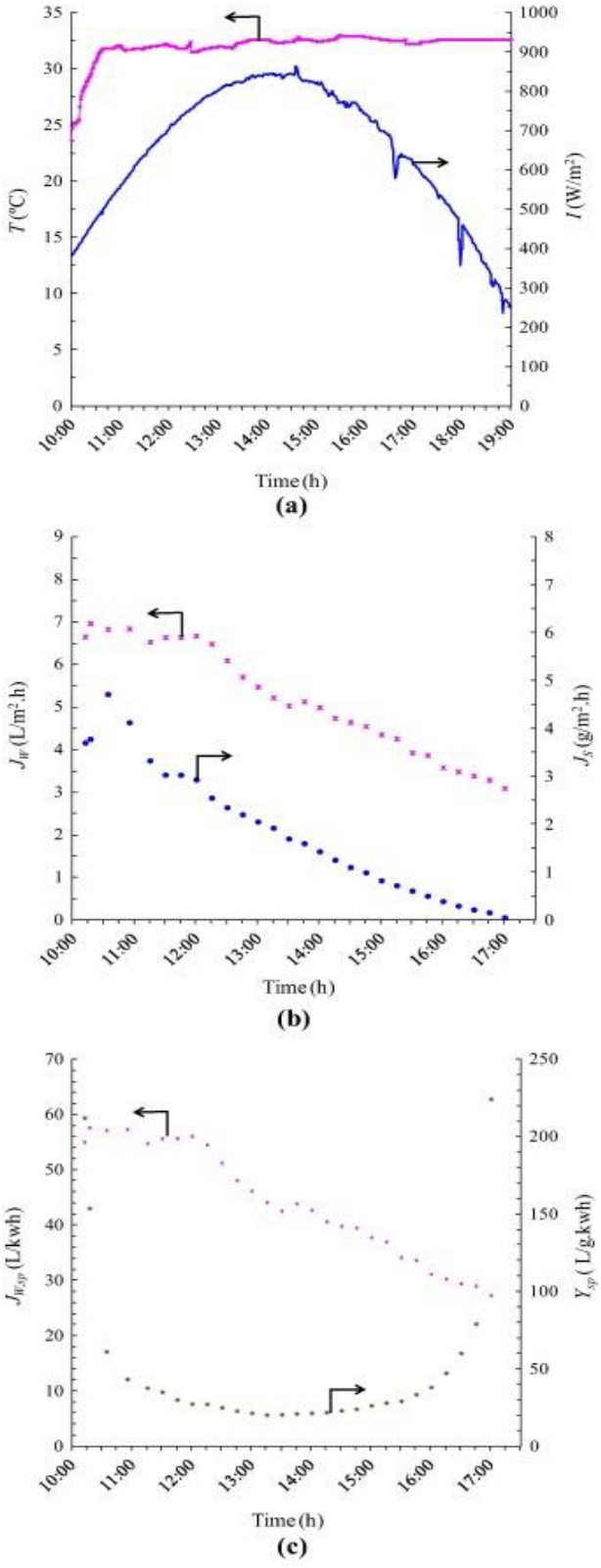

Fig. 10. Evolution of: (a) Temperature (T) and instantaneous global solar radiation on horizontal plane (I) with time, (b) obtained responses J_W and J_S, and (c) obtained responses $J_{W,sp}$ and Y_{sp} of the solar FO pilot plant.

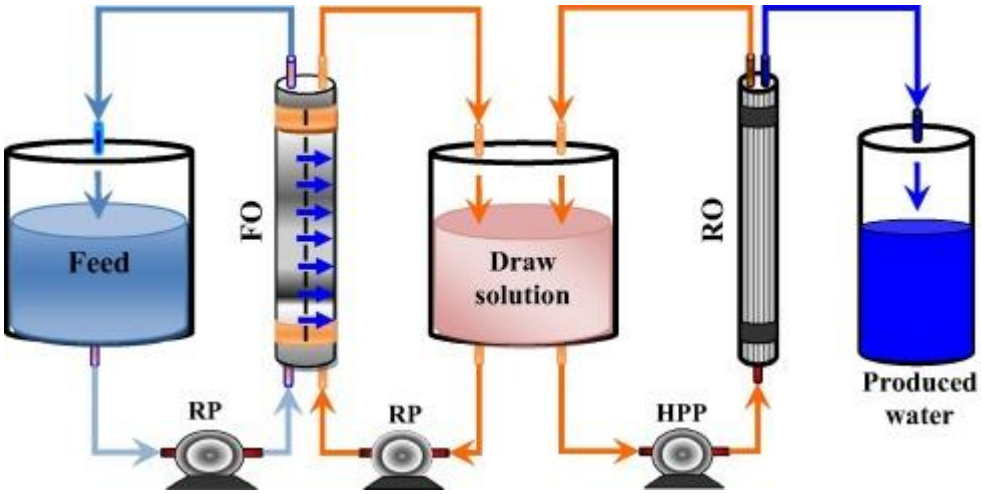

Fig. 11. FO/RO simplified schema for regeneration of the draw feed solution (RP: circulation pump, HPP: high pressure pump).

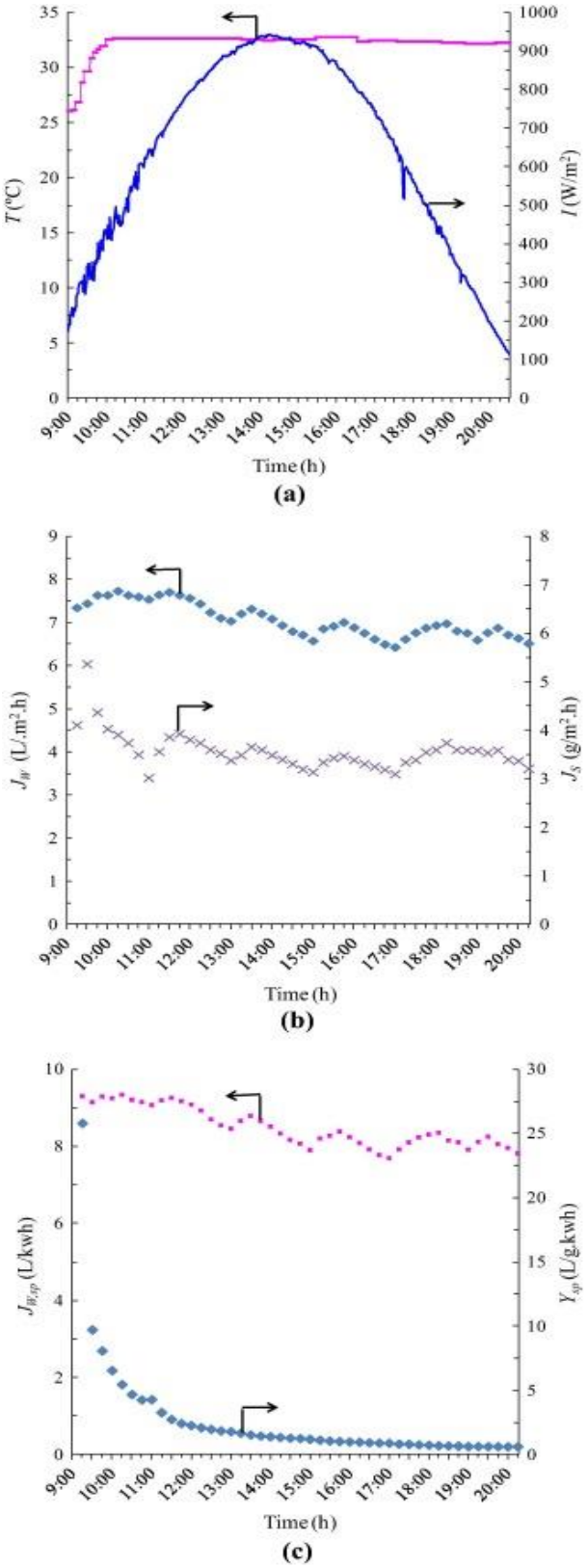

Fig. 12. Evolution of: (a) Temperature (T) and instantaneous global solar radiation on horizontal plane (I) with time, (b) obtained responses J_W and J_S, and (c) obtained responses $J_{W,sp}$ and Y_{sp} of the solar FO/RO hybrid pilot plant.

LIST OF TABLES:

Table 1. Actual and coded values of the independent variables used for the experimental design of the solar powered FO pilot plant.

Variable	Symbol	Real values of coded levels				
		$-\alpha^a$	−1	0	+1	$+\alpha^a$
ϕF (L/min)	x1	0.050	0.121	0.450	0.779	0.850
ϕP (L/min)	x2	0.050	0.094	0.300	0.506	0.550
T (°C)	x3	20.07	22.00	31.00	40.00	41.94

A $\alpha = 1.215$ (star or axial point for orthogonal CCD in the case of 3 independent variables).

Table 2. CCD experimental design (DoE) used to model the solar powered FO pilot plant and the obtained responses.

Run number and type[a]		Design factors						Responses					
		ϕ_F (L/min)		ϕ_P (L/min)		T (°C)		J_W	J_S	J_W/J_S	E_c	$J_{W,sp}$	Y_{sp}
N		x_1[b]	ϕ_F (L/min)	x_2[b]	ϕ_P (L/min)	x_3[b]	T (°C)	(L/m² h)	(g/m² h)	(L/g)	(kW h)	(L/kW h)	(L/g kW h)
1	O1	+1	0.779	+1	0.506	+1	40.00	5.77	2.89	1.996	1.081	7.47	1.846
2	O2	−1	0.121	+1	0.506	+1	40.00	4.63	3.08	1.504	1.079	6.01	1.394
3	O3	+1	0.779	−1	0.094	+1	40.00	5.19	2.97	1.745	1.080	6.73	1.616
4	O4	−1	0.121	−1	0.094	+1	40.00	4.50	3.43	1.311	1.304	4.83	1.005
5	O5	+1	0.779	+1	0.506	−1	22.00	3.98	2.99	1.334	2.119	2.63	0.629
6	O6	−1	0.121	+1	0.506	−1	22.00	3.33	3.20	1.042	2.069	2.26	0.504
7	O7	+1	0.779	−1	0.094	−1	22.00	4.19	3.09	1.355	2.185	2.69	0.620
8	O8	−1	0.121	−1	0.094	−1	22.00	3.55	3.53	1.004	2.231	2.23	0.450
9	S1	+α	0.850	0	0.300	0	31.00	5.64	3.11	1.812	0.582	13.55	3.111
10	S2	−α	0.050	0	0.300	0	31.00	4.87	3.62	1.346	0.584	11.69	2.306
11	S3	0	0.450	+α	0.550	0	31.00	4.42	2.68	1.651	0.800	7.73	2.064
12	S4	0	0.450	−α	0.050	0	31.00	4.16	3.03	1.374	0.584	9.98	2.351
13	S5	0	0.450	0	0.300	+α	41.94	6.06	3.25	1.866	1.284	6.60	1.453
14	S6	0	0.450	0	0.300	−α	20.07	4.11	3.18	1.290	2.032	2.83	0.635
15	C1	0	0.450	0	0.300	0	31.00	5.11	3.14	1.627	0.593	12.06	2.745
16	C2	0	0.450	0	0.300	0	31.00	5.12	3.13	1.633	0.584	12.26	2.795

A O = orthogonal design points, C = center points, S = star or axial points.
B −1 = low value, 0 = center value, +1 = high value, +/−α = star point value.

Table 3. Analysis of variance (ANOVA) for the developed RSM model of J_W.

Source	DF[a]	SS[b]	MS[c]	F-value	F-tab	R^2	R_{adj}^2
Model	9	9.017826	1.00198	38.206	3.8	0.9828	0.957
Residual	6	0.157356	0.02623				
Total	15	9.175182					

A *DF* - degree of freedom.
B *SS* - sum of squares.
C *MS* – mean square.

Table 4. Analysis of variance (ANOVA) for the developed RSM model of J_S.

Source	DF[a]	SS[b]	MS[c]	F-value	F-tab	R^2	R_{adj}^2
Model	9	0.812429	0.09027	24.645	3.8	0.9737	0.934
Residual	6	0.021977	0.0036628				
Total	15	0.834406					

A *DF* - degree of freedom.
B *SS* - sum of squares.
C *MS* – mean square.